European Water 89: 1-13, 2025.

The gradient of thermal potential in urban area with BME-case of I-Lan plain

Po-Chia Chen[1], Kuo-Chen Ma[2*], Mo-Hsiung Chuang[2] and Shi-Ting Fang[1]

[1] *Department of Bioenvironmental Systems Engineering, National Taiwan University, No. 1, Sec. 4, Roosevelt Rd., Taipei 10617, Taiwan*
[2] *Department of Urban Planning and Disaster Management, Ming Chuan University, No. 5, De Ming Rd., Gui Shan District, Taoyuan City 333, Taiwan*
[*] *e-mail: kcma@mail.mcu.edu.tw*

Abstract: The I-Lan Plain, situated in northeastern Taiwan at the southwestern extremity of the Okinawa Trough, is a highly urbanized region rich in low-carbon and green energy resources. The I-Lan Plain intersected by thick sedimentary layers is clipped by the special geological conditions. The area's abundant hot springs and high thermal gradients might be attributed to magmatism linked to the back-arc spreading of the Okinawa Trough. The presence of numerous hot springs in and around the I-Lan Plain indicates a high thermal gradient beneath the area. The I-Lan plain area, therefore, has the most potential thermal and sustainable energy in the important urban area of Taiwan, and has been assigned as the major energy program by local government on exploring and developing thermal power in the future. The present study examines thermal gradients on the I-Lan Palin, Taiwan. Uncertainties and spatial heterogeneities in the TG attribute are addressed via a stochastic analysis of the problem. Available information includes 2 datasets that form the analysis dataset, where both hard exact values and uncertain soft intervals are present. The Bayesian maximum entropy method (BME) is used to consider uncertainty of thermal gradient (TG) and to predict where high potential of thermal has. The BME approach provides uncertainty measures that can be used to examine potential improvement in the uncertainty. Predicting TG across the I-Lan Plain, thermal gradient values have been made available for every location on the prediction output grid. Through a separate analysis based on BME simulation has been able to produce a map that precisely identifies high thermal potential.

Key words: Bayesian maximum entropy; thermal gradient; thermal energy; soft data.

1. INTRODUCTION

Heat transfer has long been a central topic in thermodynamics, energy engineering, and geoscience. It governs the mechanisms of conduction, convection, and radiation that control temperature distribution within geological formations. In geothermal systems, heat transfer processes are influenced by rock thermal conductivity, groundwater movement, and magmatic heat sources (Yang, 2013). Quantitative modeling approaches, such as finite-element and inverse-parameter estimation methods, have been widely applied to assess subsurface heat flow and temperature distribution (Tony et al., 2008). Despite advances in numerical heat-flow modeling, conventional deterministic methods often face limitations in accounting for spatial uncertainty and data incompleteness (Lin et al., 2004; Hou et al., 2009). In regions such as the I-Lan Plain, where thermal measurements are sparse and heterogeneous, probabilistic and data-assimilation methods provide a more robust framework for temperature prediction. The Bayesian Maximum Entropy (BME) framework (Christakos, 2000) offers an integrative approach that combines physical models, statistical inference, and heterogeneous data sources to estimate spatiotemporal fields under uncertainty. BME has been successfully applied in hydrogeology, environmental modeling, and thermal field mapping (Christakos, 2004 and 2005). By assimilating both hard and soft data, it allows for non-Gaussian and nonlinear estimation of thermal gradients, making it particularly suitable for geothermal environments like the I-Lan Plain. The advanced progress and global momentum for promoting renewable energy sources is steadily increasing. Thermal energy is one such green and low-carbon energy resource and it offer a dual advantage of being cost-effective and

efficient (Fridleifsson, 2001; Lund et al., 2005; Yang, 2013). The study of heat transfer is also crucial in various fields, including physics, precision engineering, and industrial mechatronics applications (Gizem, 2019; Ku, 2019).

This study presented a geostatistics and space-time statistics method to predict the high thermal potential area. The Bayesian Maximum Entropy theory (BME) was first introduced by Christakos in 1990 (Christakos, 1990). Later on, the BME approach was adapted within a broader epistemic framework and successfully utilized to address real-world challenges in diverse scientific and energy-related domains. In order to consider the uncertainty characterizing systems in real world, this study involves BME method to be a solution. The BME methods have been specifically devised for investigating random fields characterized by non-Gaussian multivariate densities. The BME approach assumes that a physical model captures incomplete environmental knowledge about nature and emphasizes quantitative formulations of teleological reasoning and evolutionary data assimilation for the real-world system (Christakos, 1990, 1991). The factorial concept relies on representing the multivariate probability density through the product of univariate densities along with an associated set of orthogonal polynomials. Under real-world uncertainty conditions, the BME produces non-Gaussian multivariate densities by combining fundamental knowledge (natural laws, scientific theories, and theoretical space-time correlation models) with various sources of case-specific information (exact measurements, uncertain data, and secondary information). Moreover, the BME method is capable of generating informative space-time maps and images that remain valid under highly general circumstances. In this paper, we introduce the generalized BME approach, which we believe to be a potent fusion of the space-time heterogeneity found in urban areas, the structural dependence properties of the generalized random field theory, and the knowledge assimilation, non-Gaussian, and nonlinear estimation capabilities of the BME method discussed earlier. The generalized BME proves to be versatile for analyzing, modeling, and mapping a wide range of space-time attributes exhibiting heterogeneous space-time patterns and dependence structures. It excels in handling conditions of multisource uncertainty, encompassing various epistemic, physical, and technical sources, such as incomplete information, natural variation, and imperfections in measurement apparatus.

The proposed data analysis for this problem aims to answer the following scientific questions, posed as research goals for the study: (a) How can uncertainty in the study of TG in the I-Lan Plain be addressed/eliminated? (b) Can temperatures be predicted across the Plain? In higher depths? (c) Which locations can be identified as having high thermal potential? TG is sampled at depths up to about 300 m. For [B], it is desired to predict temperatures at larger depths at about an order of magnitude larger than sampling depths. The present study aims to apply the Bayesian Maximum Entropy (BME) method to analyze the thermal gradient (TG) distribution in the I-Lan Plain and to address three major scientific questions. The scope of this paper encompasses data acquisition, BME-based modeling, and spatial analysis of TG to characterize the geothermal structure of the I-Lan Plain. Furthermore, BME predictions demonstrate that temperatures can be extrapolated to greater depths with quantifiable confidence levels, offering valuable insights for geothermal exploration and sustainable energy development in northeastern Taiwan. The study presents a problem where natural uncertainty exists in the attribute TG. As such, we tackle our goals by using stochastic analysis. In the context of stochastic analysis, the TG attribute is considered as a spatial random field, that is, a collection of random variables that cover the I-Lan Plain and express TG at every location. We aim to reach the above goals by employing geostatistical methodologies to study the TG field. Specifically, we apply the Bayesian maximum entropy predictive technique. Further on, geostatistical simulation is used to study TG characteristics that can help us answer which locations can be identified as having high thermal potential.

As a secondary goal, one would like to associate TG values to amounts of electricity. Yet, the scope of present study lacks entirely any related information and input. It is suggested that additional literature and/or analytical work is needed in the context of a separate study, so that (i) relevant knowledge bases can be assessed and collected for that goal, and (ii) an analysis can substantiate how TG values could translate into a different attribute. This future analysis can be

aided by the results of the present study.

2. MATERIALS AND METHODS

2.1 Study area

The I-Lan Plain is the most important urbanized area and lies on the northeastern coast of Taiwan, and hosts the city of I-Lan in the I-Lan County (Figure 1). The plain intersected by thick sedimentary layers is clipped by the special geological conditions. The plain is bounded by major geological structures. The area's abundant hot springs and high thermal gradients might be attributed to magmatism linked to the back-arc spreading of the Okinawa Trough. It is a subsiding graven-like depression filled with Quaternary fluvial and marine sediments that overlie Neogene volcanic and sedimentary basement rocks. The region is characterized by intense crustal deformation due to the interaction between the Eurasian Plate and the Philippine Sea Plate. Continuous extensional tectonics associated with the back-arc spreading of the Okinawa Trough has resulted in high geothermal gradients and vigorous hydrothermal activity across the plain. These processes have generated numerous hot springs distributed mainly along fault zones and uplifted areas. In addition, the thick sedimentary cover—composed of clay, silt, sand, and gravel layers—acts as both a heat reservoir and a cap rock system that retains geothermal fluids.

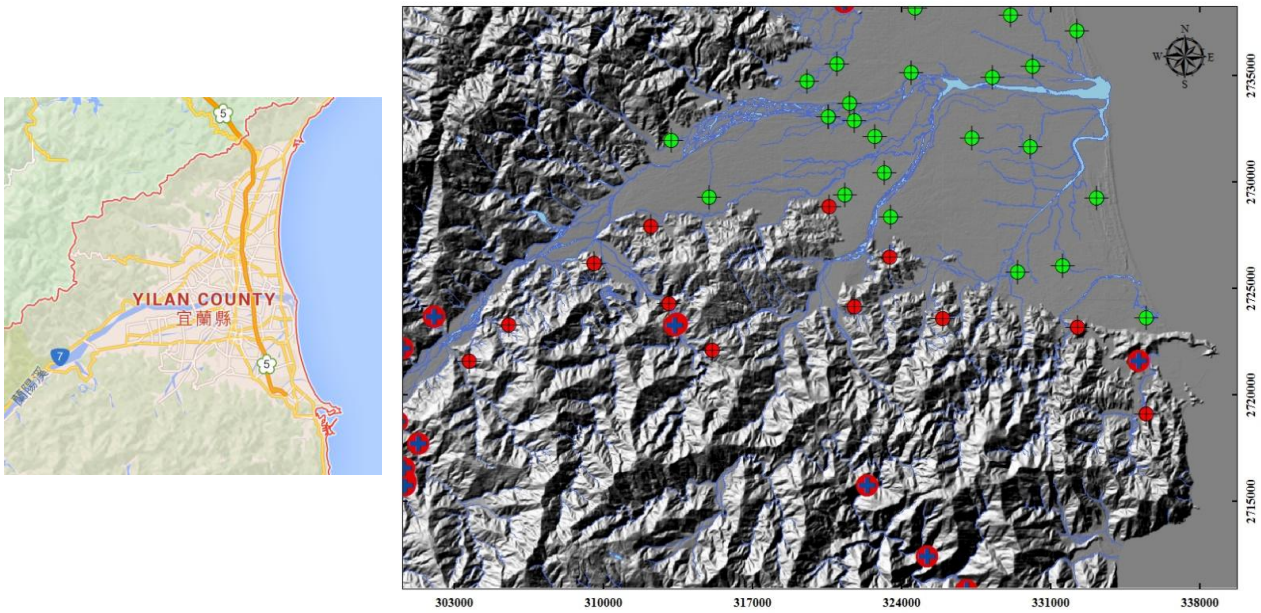

Figure 1. I-Lan Plain, Taiwan (Source: Google Maps and Liu, et al., 2012).

According to investigations conducted by the Industrial Technology Research Institute (ITRI), the thermal field in the I-Lan Plain appears to be one of the most suitable areas for developing sustainable energy within Taiwan's urbanized regions. In 1981, an experimental thermal power plant was constructed within this thermal field; however, the plant was shut down and closed after 11 years because of the shortage of the operational funding. After the stage of following exploitation surveys, the ITRI constructed nineteen deep production wells with commercially successful wells confined to a smaller and fine-grid area at the urban zone. Although the distribution of the sustainable energy in this urban area has been investigated previously (Cheng and Lee, 1977; Su, 1978; Tseng, 1978; Hsiao and Chiang, 1979; Chiang and Liu, 1983), the configuration of the thermal reservoir has not yet been accurately described. This finding could inform the design of new production wells for energy utilization in urban areas, taking into account

the optimal locations and trajectories of boreholes within the reservoir. The primary objective of this study is to sketch the thermal energy spatial distribution of this urban area by integrating geophysical data and borehole information. For this, geomagnetic and gravity description datasets obtained in the I-Lan Plain underwent reprocessing and interpretation. Furthermore, additional magnetotelluric (MT) data and well information were incorporated to develop the thermal conceptual model for the urban plain area in this study. We are interested in studying the thermal temperature gradient in the area. The available information is a series of Thermal Gradient (TG) measurements across the Plain.

2.2 The thermal gradient datasets

The I-Lan Plain TG dataset comprises of 2 separate datasets, A and B. All data are expressed in the TWN97 datum, where coordinates are in Easting and Northing and distances are measured in meters (m). Dataset A has 38 records with columns of coordinates and TG values. Dataset B has 30 records of coordinates, well depth, measurement depth, temperature, heat flow, and TG values.

TG is measured in °C/100m and can take both positive and negative values. The attribute depends on depth. However, dataset A has no depth information, and the number of records in dataset B are too few for geostatistical analysis to investigate TG spatial correlation in 3 dimensions (that is, the 2 planar dimensions and depth). These conditions mandate that our study be conducted in the 2-dimensional horizontal plane, whereby TG is considered depth-independent. For dataset B, each borehole record contains temperature measurements at different depths, along with calculated heat flow and thermal gradient (TG) values. To ensure consistency with dataset A, which lacks depth information, the TG values used from dataset B were derived from the available measurement intervals within each borehole. When multiple temperature–depth data points were available for a single location, an *average TG value* was computed based on the linear temperature gradient between the shallowest and deepest recorded depths. This averaging approach minimizes localized fluctuations and provides a representative TG value for each site that reflects the overall vertical thermal trend within the upper 300 m of the subsurface. That is, at any location on the I-Lan Plain, a TG value is assumed to be valid for the entire column of soil underneath.

2.3 Missing and extremes values

The datasets A and B have no missing values and have an initial count of 68 records. In an initial statistical inspection, given the mean m and the standard deviation σ of the aggregated dataset, we deemed the values that lie outside the interval $[m-3\sigma, m+3\sigma]$ as potential extreme values. TG values from Dataset A were identified as statistical outliers (Figure 2). However, these data points were retained in the analysis because expert evaluation confirmed their reliability and geological plausibility. Including them ensures that naturally occurring thermal anomalies are represented in the spatial analysis rather than being mistakenly excluded as sampling errors.

2.4 Duplicates analysis

The I-Lan Plain TG data are also checked for duplicate records. Duplicates are defined as any 2 or more records that have the exact same coordinates (collocated). Dataset B was found to contain no duplicate records. However, in Dataset A, 4 groups of duplicate records were found. The observation numbers of the duplicates are as follows:

(a). 7, 8 : Records have identical TG value 4.2 °C/100m. Might be a data entry error.
(b). 15, 23 : Records have very similar gradient values (3.3 and 3.7 °C/100 m)
(c). 3, 11, 12: Records have very similar gradient values (1.8723, 1.71, 1.68 °C/100 m)
(d). 9, 10 : Records have unusually different values (25.6838 and 0.8797 °C/100 m)

Case (a) is trivial. We can safely ignore one of the 2 records in the analysis. Cases (b) and (c) have neighboring TG values. Each group is reduced to a single interval soft datum at that location, where the lower limit is assumed to be the lower of the group values, and the upper limit is assumed to be the higher of the group values. Case (d) resembles the previous case of (b) and (c) except for the fact that the group features a pair of TG values that differ significantly in the context of the data range in the present study (see Table 1). Expert feedback stated that both values in group (d) are valid, and were sampled at locations so neighboring that the same coordinates were assigned to both of those records. In the datasets, distances are measured in m and coordinates are specified with 2 decimal digits. Since the coordinate's accuracy is in the order of centimeters, the expert feedback suggests that both measurements were taken within a centimeter of each other. While not impossible, this statement suggests a spatially extremely heterogeneous field of TG values that the present analysis is unable to study at the centimeter spatial scale. We honor the expert feedback by treating the collocated records of group (d) exactly like the collocated record groups (b) and (c) above. That is, records (d) were also reduced to a single interval soft datum that was defined in the exact same manner as in the cases (b) and (c) above.

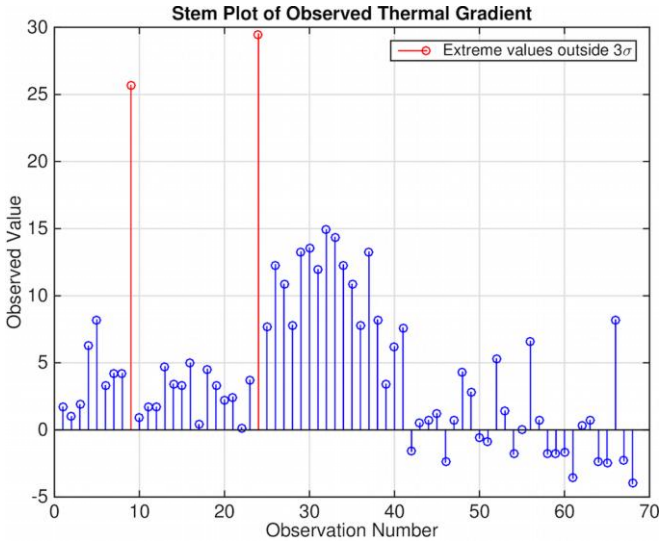

Figure 2. Stem Plot of the I-Lan Plain Dataset. Extreme Values Shown in Red Stems.

2.5 Working dataset

After addressing the duplicate records, the resulting dataset for the TG analysis comprises 60 observations, out of which 57 are hard data and 3 are interval soft data. Some basic dataset statistics are shown in Table 1. The data locations and the color plot of the data values are shown in Figure 3. A histogram of the data distribution is shown in Figure 4. The histogram indicates that the majority of TG values lie between -4 °C/100 m and 15 °C/100 m, and also illustrates the extreme values that occupy the remote isolated bin of values between 26-30 °C/100 m.

Table 1. Basic statistics for the I-Lan Plain TG dataset.

Measure	Value
x-axis sample span, span width (m):	[300,272.00, 335,488.40] , 35,216.4
y-axis sample span, span width (m):	[2,715,731.00, 2,751,313.12] , 35,582.12
Sample min value (°C/100m):	-4
Sample max value (°C/100m):	29.5
Sample Mean (°C/100m):	4.4615
Sample Standard Deviation (°C/100m):	6.0727
Skewness:	1.3184
Kurtosis:	5.8372
Mode (°C/100m):	0.7
Median (°C/100m):	3.33

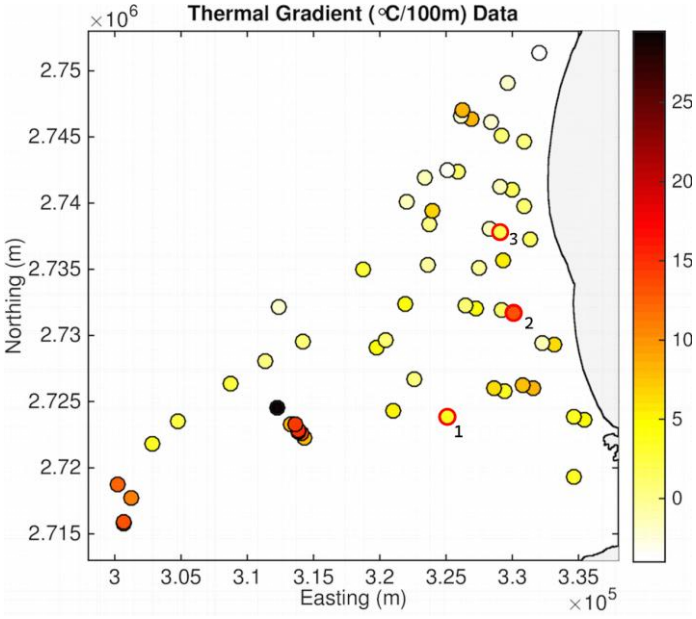

Figure 3. Color Plot of the I-Lan Plain TG Dataset. Soft intervals are represented by the interval mean. Data points 1, 2, and 3 are soft data, whereas all other points are considered hard data.

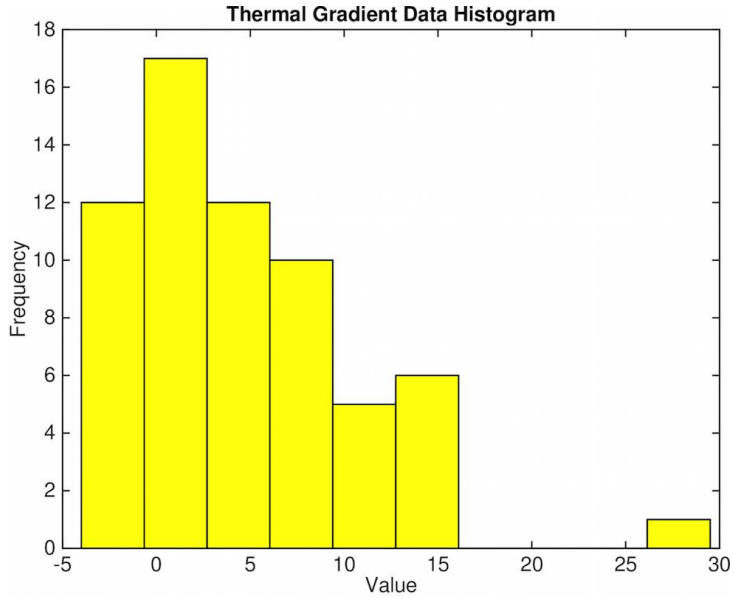

Figure 4. Histogram of the I-Lan Plain TG Dataset.

3. UNCERTAINTY, TREND ANALYSIS AND CORRELATION

In the following step we study spatial variability in the I-Lan Plain TG data. Investigating spatial variability can help us reveal spatial correlation patterns and underlying behavior mechanisms in the TG field, which are critical for prediction and simulation tasks.

An inspection of Figure 3 shows no visible TG value trends in any spatial direction across the I-Lan Plain. That is, all observations appear to be within a specific range of values across the Plain without exhibiting organized spatial patterns of value change. Instead, there exist only some isolated areas of higher values to the south and southwest of the Plain that do not warrant trend behavior. In geostatistical analysis it is desirable to remove spatial trends before investigating correlation, because they indicate variability in higher spatial scales that can overshadow study of variability in the study spatial scale. On the basis of the assessment about apparent lack of trends in the TG values spatial distribution, the trend removal task can be skipped in the present case.

We then proceed to study how TG values are correlated in space. The correlation analysis has 2 different stages. First, we use the TG observations to form all possible pairs among them. By quantifying the spatial similarity of the pair's values at different distances, we produce an empirical estimate of the correlation behavior in the TG dataset. We express the spatial similarity by means of the covariance value from each pair of TG observations. Figure 5 shows the empirical estimate of spatial covariance for the I-Lan Plain TG data at a few selected lag distances designated by the red circles. The empirical covariance plot shows that correlation starts from the maximum value of the dataset variance at zero distance. As the distance between pairs increases, correlation drops between observations separated by larger distances. Understanding this behavior is very important, because it shows us essentially how far away from any observed value we might be able to infer TG values.

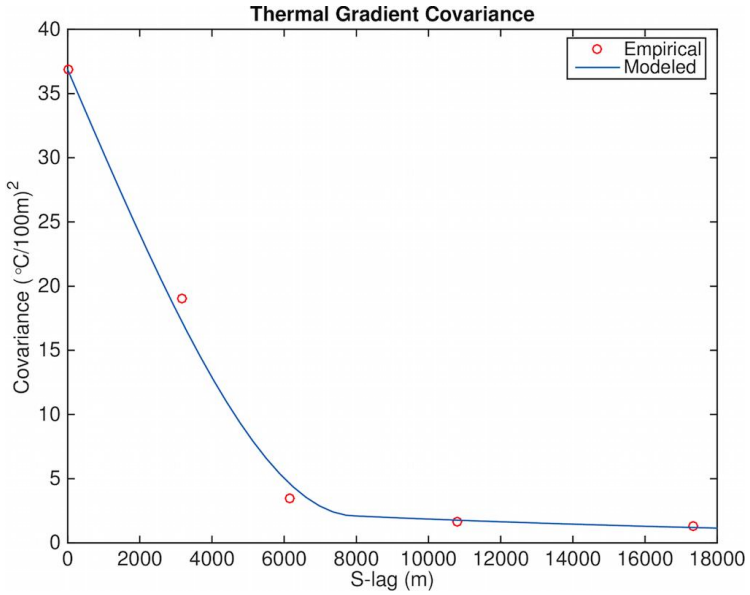

Figure 5. Empirical and Fitted Covariance for on I-Lan Plain TG.

The second stage in correlation analysis is to model the empirical behavior by fitting an appropriate mathematical function to the empirical covariance values. A model can then provide a covariance value between any arbitrary pair of locations across the I-Lan Plain. Subsequently, this knowledge can help us predict TG at a location where there is no sampled value: We can simply use the fitted covariance model to associate the values at sampled neighboring locations with the unknown value at the prediction location.

Mathematical conditions stipulate that only positive-definite functions can be used as covariance models. Commonly used covariance models are formed by considering basic functional forms like the Gaussian, exponential, and spherical form. One or more such functional forms can be used to build covariance models with one single or multiple nested component structures. In general, a covariance model has a sill parameter that expresses the maximum covariance accounted for by the model, and a range parameter that shows the spatial distance this model extends to. The solid line in Figure 5 shows the model fitted to the empirical covariance of the I-Lan Plain TG data. This is a nested model with a spherical component and an exponential component; it depends on the distance r (unit is meter) between any 2 locations, and is described by the following expression:

$$C(r) = \begin{cases} c_1\left[1 - 1.5\left(\frac{r}{r_1}\right) - 0.5\left(\frac{r}{r_1}\right)^3\right] + c_2 exp\left(-\frac{r}{r_2}\right), r < r_1 \\ c_1 + c_2 exp\left(-\frac{r}{r_2}\right), r_1 \le r \end{cases} \quad (1)$$

where $c_{1+}c_2$ is the total TG variance (assumed to be approximated by the sample variance which is inferred as about 36.88 [°C/100 m]^2; see Table 1). The values of the fitted model parameters are

presented in Table 2.

Table 2. Covariance model component structures and parameters for the I-Lan Plain TG field.

Nested Structure i	Model	Sill c_i (°C/100m)^2	Range r_i (meter)
1	Spherical	33.50	7,900
2	Exponential	3.38	50,000

The fitted model offers us insight about the spatial correlation behavior of the TG values on the I-Lan Plain. The dominant spherical component accounts for most of the total TG variance, and its range has been estimated to 7.9 km. The exponential component contributes with a sill of about less than 10% of the total variance, and its influence appears to extend to a range of 50 km, that is, farther out than the area of interest that is the I-Lan Plain. In the following, these components jointly enable us to predict TG at unsampled locations, and to later also simulate the TG field.

Up to this point, the analysis has provided a detailed answer to goal [A] in Section 1 of this report. Uncertainty in TG on the I-Lan Plain is comprehensively addressed by means of stochastic analysis and statistical description of the attribute TG characteristics as a spatial random field. Uncertainty cannot be eliminated due to (i) inherent natural uncertainty in TG, and (ii) our inability to account for all factors that affect the TG spatial behavior. However, through stochastic analysis not only can we assess TG, but we can also express a level of certainty about this assessment up to the degree of our statistical confidence. This becomes more apparent in the next section where we investigate prediction of TG at unsampled locations.

4. SPATIAL PREDICTION

The covariance analysis provided us with means to describe how the TG values change with spatial distance on the I-Lan Plain. To this finding, we will add the given hard and soft TG measurements to produce a set of predicted TG values across the I-Lan Plain. In the Bayesian maximum entropy (BME) context, we now want to conditionalize the prior general knowledge of spatial correlation behavior upon the case-specific knowledge of the TG values at the sample locations. The BME theory provides this facility, and produces a posterior probability density function (PDF) at every specified prediction location.

We select a network of locations to be the prediction locations across the I-Lan Plain. Specifically, we define a rectangular output grid that has a rather dense network of 81 equally spaced nodes in each direction. The entire grid spans a square area of 40,000 m by 40,000 m, hence the distance between any two neighboring nodes in the horizontal or vertical direction is 500 m. In spatial prediction, each node is assigned a TG value on the basis of the values of the nearest neighboring measurement locations, and the covariance model that correlates the node with its neighbors.

The result is a predicted posterior PDF at each output grid node. Revisiting the analysis input, the TG dataset provides us with the first 2 statistical moments of the TG field on the I-Lan Plain; that is, the (assumed constant) TG mean and the TG covariance. Statistics mandates that this input produces Gaussian posterior PDFs, which can be fully described by their mean and variance parameters. In line with this approach, BME prediction yields the BME mean and variances of the TG posterior PDFs at all output grid locations across the I-Lan Plain.

The predicted BME mean values of TG are illustrated in Figure 6. Observe that TG is expected to range within generally low values between 0 and 5 °C/100m. There exist patches of lower and higher values in accordance with the observed data. The blank triangular area in the northwest corner of the plot are missing values, where inference is not possible. This effect is due to the covariance model range, and the entire lack of measurements in that neighborhood that could contribute to prediction (compare Figure 6 to Figure 3 that presents the data locations on the I-Lan Plain).

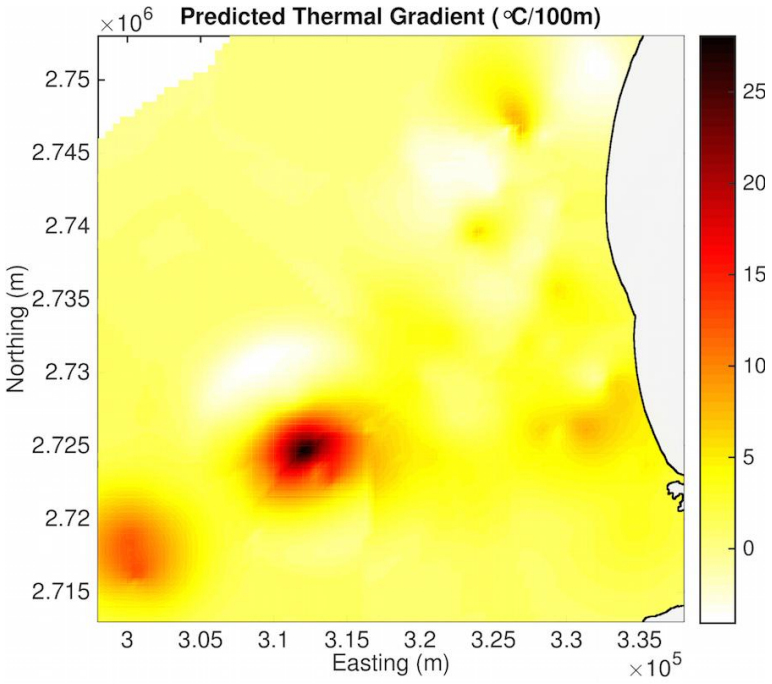

Figure 6. BME mean of predicted TG across the I-Lan Plain.

By examining Figure 6, one might be inclined to address research goal outlined in Introduction namely, whether the high TG values observed in the southwestern portion of the I-Lan Plain could indicate zones of elevated thermal potential. While Figure 6 appears to support this possibility, the simulation analyses presented in the following section provide a more definitive evaluation of question.

Finally, Figure 7 quantifies the uncertainty in the prediction of TG across the I-Lan Plain. The plot shows a map of the standard error in the TG prediction at every node of the output grid. The map indicates plausibly that prediction error is minimal at the data locations, and gradually increases at locations that are progressively more distanced from the data. The highest error values reach about 6 °C/100m, and this indicates less dependable prediction in data-sparse areas of the I-Lan Plain.

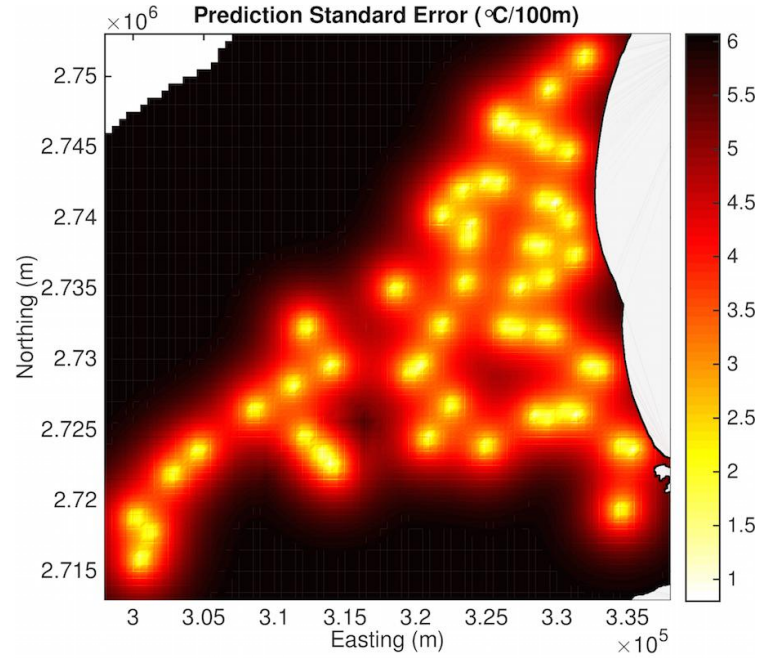

Figure 7. BME standard error of predicted TG across the I-Lan Plain

5. RESULTS AND DISCUSSION

With spatial simulation, it is possible to create realizations of the TG field in a way that both the TG filed mean and its correlation structure are preserved. Specifically, we apply conditional Gaussian simulation that honors the observed hard and soft data of the TG dataset. Any single realization is a possible snapshot of the TG values across the entire I-Lan Plain. In the following, we run a simulation of the TG field with 5,000 realizations. We simulate TG at the same locations of the output grid defined in the previous part. Figure 8 shows selected realizations from this simulation. Individual realizations can help us explore potential different views of the TG field, based on the given TG field characteristics. However, a simulation can be even more useful when one analyzes the aggregated set of all realizations to extract statistics about the expected TG behavior.

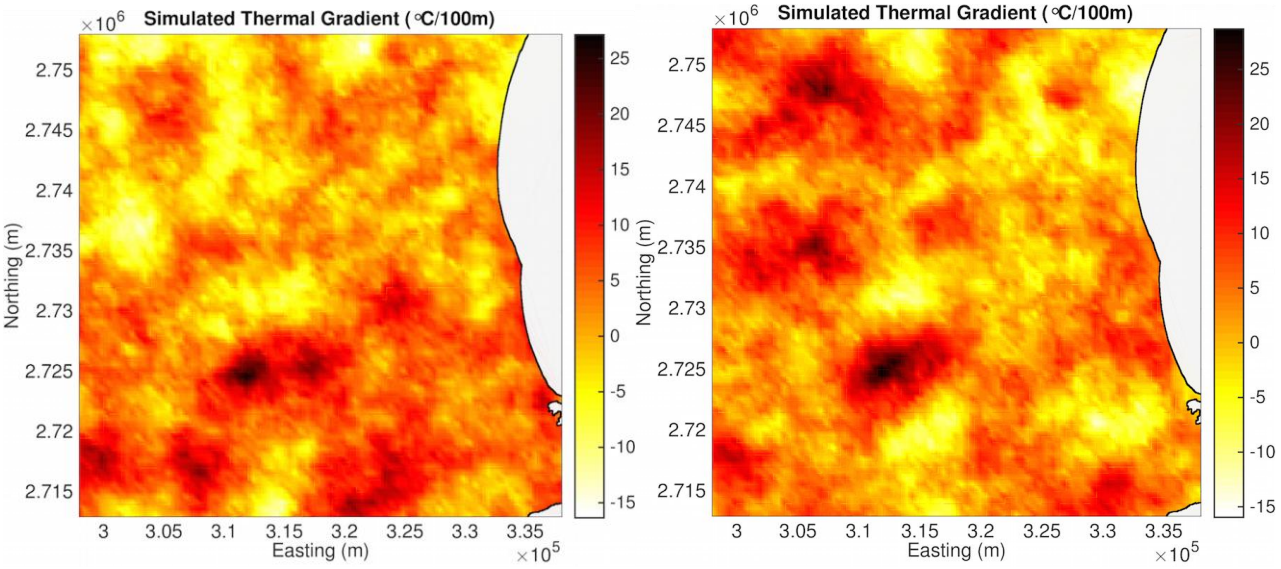

Figure 8. Selected realizations from Gaussian conditional simulation of TG across the I-Lan Plain. The pictured realizations correspond to simulation iterations 739 and 2754.

In Figure 2, it was remarked that almost all TG values in the I-Lan Plain dataset are lower than 15 °C/100m, except for the 2 extreme values indicated in Figure 2. It would make a sensible step in our analysis, then, to consider that locations where TG exceeds the threshold value TGThr = 15 °C/100m are suitable high thermal potential candidates. We proceed to address our goal with the following 2 steps.

In the first step, we want to compute the percentage of locations on the I-Lan Plain that is expected to exceed the threshold value TG_{Thr}. For each one of the 5,000 realizations in the simulation task, we compute the number of locations where the simulated TG $\geq TG_{Thr}$. The count of those locations across all realizations is the number N_{ExcThr} of all locations that exceed the threshold value TG_{Thr} in the entire simulation task. The number of locations where simulated values are computed in the entire simulation task is N_{all} = 81×81 (output grid nodes) × 5,000 (number of realizations) = 32,805,000 nodes in total. Then, the ratio N_{ExcThr}/N_{all} is the percentage we seek for. The analysis shows that N_{ExcThr}/N_{all} = 554,113/32,805,000 = 0.016891 or 1.6891%.

That is, about 1.69% of all locations on the I-Lan Plain can be expected to exceed the threshold value TG_{Thr}, and are therefore suitable high thermal potential candidates. Further analysis shows that in the 95% confidence interval, this percentage is expected to range between the percentages values [1.67, 1.71]. This result is visually illustrated in Figure 9, where the plot shows the percentage of values that exceed TG_{Thr} in each one of the 5,000 realizations. Interestingly, the plot indicates there existed several of the 5,000 realizations in which as much as about 5% of the locations exhibited TG values in excess of the threshold TG_{Thr}.

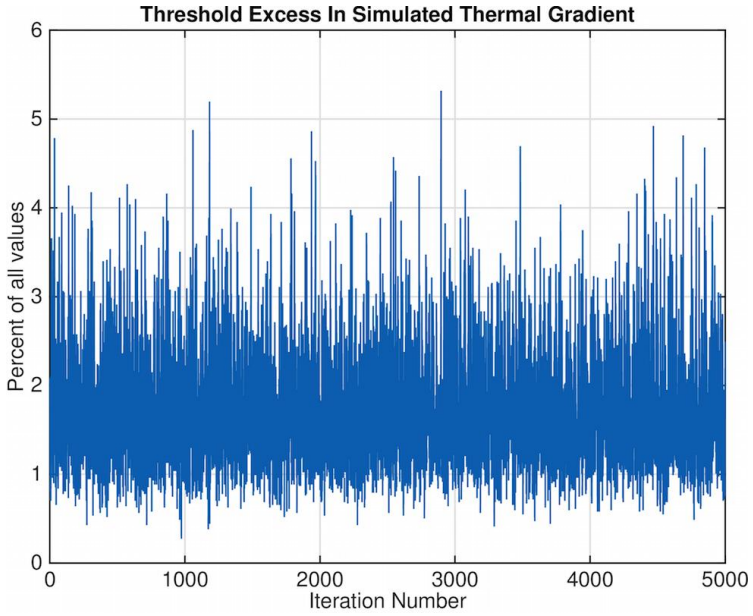

Figure 9. Percentage of values that exceed TGThr in each one of the 5,000 realizations.

In the second step, we want to identify these high thermal potential locations on the I-Lan Plain. To do so, this time we perform an averaging of the simulated values that exceed TGThr with respect to each individual location of the total 81×81 = 6,561 locations on the I-Lan Plain grid. For each location, the percentage of realizations where TGThr was exceeded over the course of 5,000 realizations is the probability that this location is a suitable high thermal potential candidate, as defined earlier. Figure 10 shows the results of this task.

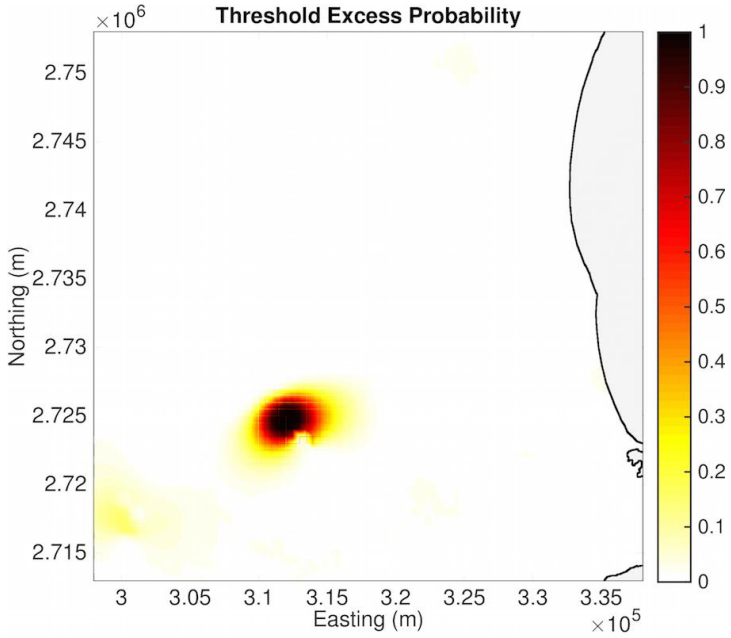

Figure 10. Probability map of high thermal potential locations on the I-Lan Plain.

According to the 5,000 realizations of the simulation task, the likeliest candidate locations to explore high thermal potential on the I-Lan Plain are situated to the southeast of the Plain. The map in Figure 10 shows, in particular, a small area to the southwest of the Plain center where the probability reaches 100%, whereas a second area of interest to the far southwest side of the Plain exhibits probabilities as high as about 25%.

6. CONCLUSIONS

The present study examines thermal gradients on the I-Lan Palin, Taiwan. Uncertainties and spatial heterogeneities in the TG attribute are addressed via a stochastic analysis of the problem. Available information includes 2 datasets that form the analysis dataset, where both hard exact values and uncertain soft intervals are present. Geostatistics is employed to (i) perform a spatial correlation analysis of TG, (ii) predict TG across the I-Lan Plain with the Bayesian maximum entropy predictive methodology, and (iii) simulate TG on the same grid across the Plain to derive specific answers to the study goals. Specifically, the goals set for this study have been stated and addressed as shown in the following.

(a) Although eliminating uncertainty is not feasible on the grounds of natural uncertainty and the finite amount of available information about TG, addressing this uncertainty has been made possible through the stochastic analysis approach that was applied in the study. Uncertainty has been addressed by quantifying it through key characteristics of the TG attribute in the geostatistical context, such as its spatial correlation structure and prediction of the TG values across the I-Lan Plain. The stochastic analysis approach provides uncertainty measures that can be used to examine potential improvement / reduction in the uncertainty, if additional information is made available for the TG field and incorporated in future studies.

(b) As a result of predicting TG across the I-Lan Plain, thermal gradient values have been made available for every location on the prediction output grid. Therefore, in the presence of temperature data that show temperatures at given depths, one can apply the thermal gradient predicted values to estimate temperatures throughout the Plain. In the present study, it was stressed that the thermal gradient data were only useful to consider for the entire column at the measurement location. Hence, predicted TG values indicate thermal gradient that is assumed to be valid for all depths at each prediction location. Given this assumption of TG height-independence, the present analysis results can be used for shallower as well as higher depths. It is noted here that a more elaborate, depth-dependent analysis of TG will require a different study with additional (higher count of) measurements with depth information, too, so that a proper 3-dimensional geostatistical analysis of TG is enabled.

(c) By suitably defining what “high thermal potential” is, a separate analysis based on geostatistical simulation has been able to produce a map that precisely identifies such locations. It is noted, that the analysis can be easily repeated, if “high thermal potential” should be redefined by means of a different threshold TG value.

REFERENCES

Christakos G., 1990. Random field modeling and its applications in stochastic data processing, Ph.D. Thesis, Applied Sciences Division, Harvard University, Cambridge, MA.

Christakos G., 1991. Some applications of the Bayesian maximum-entropy concept in geostatistics. Fundamental Theories of Physics 43: 215-229. DOI: https://doi.org/10.1007/978-94-011-3460-6_20.

Christakos G., 2005. Methodological developments in geophysical assimilation modeling, Rev. Geophys., 43, RG2001-RG2001-20. DOI: https://doi.org/10.1029/2004RG000163.

Christakos G., 2000. Modern Spatiotemporal Geostatistics. Oxford University Press, New York, 2012. New edition, Dover Public Inc., Mineola, NY.

Christakos, G., 2004. The cognitive basis of physical modelling. Developments in Water Science 55: 661-669. DOI: https://doi.org/10.1016/S0167-5648(04)80089-3.

Cheng, W. T. and C. F. Lee, 1977. Bipole-dipole resistivity mapping in the Chingshui geothermal area. Mining & Metallurgy 21: 88-93. Available at: https://twgeoref.gsmma.gov.tw/

Chiang, S. C. and Y. F. Liu, 1983. Application of TDEM method in the Chingshui geothermal area, Ilan, Taiwan. Petroleum Geology of Taiwan 19: 197–218. Available at: https://twgeoref.gsmma.gov.tw/.

Fridleifsson, I. B., 2001. Geothermal energy for the benefit of the people. Renewable and Sustainable Energy Reviews 5: 299-312. DOI: https://doi.org/10.1016/S1364-0321(01)00002-8.

Gizem E., 2019. Land selection criteria for lights out factory districts during the industry 4.0 process. Journal of Urban Management 8: 377-385. DOI: https://doi.org/10.1016/j.jum.2019.01.001.

Hou, C. S., J. C. Hu, K. E. Ching, Y. G. Chen, C. L. Chen, L. W. Cheng, S. H. Huang, and C. H. Lo, 2009. The crustal deformation of the Ilan Plain acted as a westernmost extension of the Okinawa Trough. Tectonophysics 466: 344-355. DOI: https://doi.org/10.1016/j.tecto.2007.11.022.

Hsiao, P.T., Chiang, S.C., 1979. Geology and geothermal system of the Chingshui–Tuchang geothermal area, Ilan, Taiwan. Petroleum Geology of Taiwan, 16, 205–213. Available at: https://twgeoref.gsmma.gov.tw/ (accessed 2025-11-12).

Ku, C.Y., C.Y. Liu, J.E. Xiao, W.P. Huang, and Y. Su, 2019. A spacetime collocation Trefftz method for solving the inverse heat conduction problem. Advances in Mechanical Engineering, 11: 1-11. DOI: https://doi.org/10.1177/1687814019861271.

Lund, J.W., D. H. Freeston, and T. L. Boyd. 2005. Direct application of geothermal energy: 2005 Worldwide review. Geothermics 34: 691-727. DOI: https://doi.org/10.1016/j.geothermics.2005.09.003.

Lin, J. Y., S. K. Hsu, and J. C. Sibuet. 2004. Melting features along the western Ryukyu slab edge (northeast Taiwan): Tomographic evidence. Journal of Geophysical Research – Solid Earth, 109(B12), B12402. DOI: https://doi.org/10.1029/2004JB003260.

Su, F. C., 1978. Resistivity survey in the Chingshui prospect, Ilan, Taiwan. Petroleum Geology of Taiwan 16: 255–264. Available at: https://twgeoref.gsmma.gov.tw/.

Tong, L.T., Ouyang, S., Guo, T.R., Lee, C.R., Hu, K.H., Lee, C.L., Wang, C.J., 2008. Insight into the geothermal structure in Chingshui, Ilan, Taiwan. Terrestrial, Atmospheric and Oceanic Sciences 19: 413-424. DOI: https://doi.org/10.3319/TAO.2008.19.4.413(T).

Tseng, C. S., 1978. Geology and geothermal occurrence of the Chingshui and Tuchang districts, Ilan. Petroleum Geology of Taiwan 15: 11–23. Available at: https://twgeoref.gsmma.gov.tw/.

Yang, J., 2013. Strategies for Low-Carbon Green Growth and Urban Management in Korea. Journal of Urban Management 2: 85-101. DOI: https://doi.org/10.1016/S2226-5856(18)30066-9.